Electrical Method to Quantify Nanoparticle Interaction with Lipid Bilayers

Randy P. Carney,[†] Yann Astier,[‡,§] Tamara M. Carney,[†] Kislon Voïtchovsky,[†] Paulo H. Jacob Silva,[†] and Francesco Stellacci[†,*]

[†]Institute of Materials, École Polytechnique Fédérale de Lausanne, EPFL-STI-IMX-SuNMIL, Lausanne CH-1015, Switzerland and [‡]ITQB, Universidade Nova de Lisboa, Avenida Da Republica, Oeiras, Portugal. [§]Present address: IBM Thomas J. Watson Research Center, Yorktown Heights, New York 10598, United States.

ABSTRACT

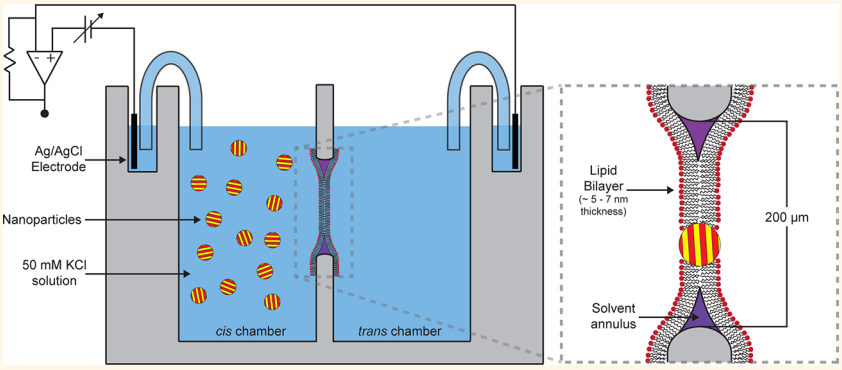

Understanding as well as rapidly screening the interaction of nanoparticles with cell membranes is of central importance for biological applications such as drug and gene delivery. Recently, we have shown that "striped" mixed-monolayer-coated gold nanoparticles spontaneously penetrate a variety of cell membranes through a passive pathway. Here, we report an electrical approach to screen and readily quantify the interaction between nanoparticles and bilayer lipid membranes. Membrane adsorption is monitored through the capacitive increase of suspended planar lipid membranes upon fusion with nanoparticles. We adopt a Langmuir isotherm model to characterize the adsorption of nanoparticles by bilayer lipid membranes and extract the partition coefficient, *K*, and the standard free energy gain by this spontaneous process, for a variety of sizes of cell-membrane-penetrating nanoparticles. We believe that the method presented here will be a useful qualitative and quantitative tool to determine nanoparticle interaction with lipid bilayers and consequently with cell membranes.

KEYWORDS: amphiphilic nanoparticles · colloidal synthesis · planar lipid bilayers · black lipid membranes · electrophysiology · endocytosis · cell membrane penetration · internalization · surface structure

The understanding of biological processes at the nanoscale is a strong driving force behind the development of nanotechnology. Small monolayer-protected nanoparticles (NPs) exist in the same size domain as proteins (~10 nm),[1] rendering them as suitable materials for a variety of biological and medicinal applications, from biomarkers/sensors to drug and gene delivery.[2−7] Gold NPs in particular have been extensively applied in biology due to their ease of synthesis and bioconjugation.[8−12] Despite these investigations, the details of their interaction with cellular machinery, particularly the cellular membrane, remain largely unknown.

Due to the potential of biomedical applications, much recent work has been directed toward the interaction between NPs and cell membranes.[13−16] Most of this research encompasses NPs in the range 10−100 nm and concludes that cells take up these NPs by one of two energy-dependent mechanisms: receptor-mediated endocytosis or transient membrane poration.[17−20] Recently however, we have discovered a type of amphiphilic gold NP coated with a mixture of ligand molecules that form stripe-like domains in their surface monolayer. These "striped" NPs spontaneously diffuse through cellular membranes into the cytosol of several types

* Address correspondence to francesco.stellacci@epfl.ch.

Received for review April 4, 2012 and accepted December 26, 2012.

Published online December 26, 2012
10.1021/nn3036304

of cells through an energy-independent mechanism.[9,21−23] We believe that striped gold NPs are a subset of a large class of nanostructured materials that are capable of fusion and penetration through lipid bilayers without overt membrane disruption. Indeed recent work from other groups suggests that cellular uptake of NPs in the 2−20 nm range is not exclusively energy-dependent.[9,21−25] In addition to size, NP surface composition,[21,22,26] ligand arrangement and patterning,[9,11,27,28] and charge[18,29,30] have each been shown to be critical for efficiency of passive entry pathways of cell penetration. Although the mechanism(s) of passive translocation for NPs remains unidentified, several groups report that NP penetration induces critical structural changes in the lipid bilayer to allow transport to the cytosol.[28,31,32] To date there is no general understanding as to what criteria a NP should have to passively penetrate membranes. This is partly due to a lack of tools that are able to methodically screen and quantify the interactions between different NPs and the same biomembrane. Here, we present such a tool, based on an electrical method to screen and quantitatively investigate the interaction between model membranes and NPs.

The complexity of the cellular membrane, especially the mechanisms that regulate membrane translocation, often renders decoupling interactions between a synthetic object and the cell membrane challenging. The cell membrane is a self-assembled structure composed mainly of lipids and constitutes a physical barrier between the cytosol and the outside world. Ionic and molecular transport into and out of the cell is largely regulated by the lipid composition and by membrane proteins working as channel or pumps.[33,34] If the flow of ions or molecules through the lipid bilayer is driven by diffusion, it is referred to as passive transport, as it requires no energy from the cell.[35,36] During this process the membrane structure controls the rate and selectivity of transported molecules.[35] Larger objects are typically taken up through facilitated passive diffusion, using channel proteins or carrier proteins, or by energy-mediated endocytotic mechanisms.[34] However, there exists a set of large proteins, cell-penetrating peptides (CPPs), that, in some cases, can translocate cell membranes through a non-energy-mediated, nonfacilitated pathway.[37,38] CPPs have been shown to enter giant unilamellar vesicles (GUVs) composed solely of model phospholipid membranes free of proteins.[1] Although their uptake mechanism remains in question, these and other results suggest that CPPs can transiently alter the local structure of the phospholipid bilayer (without forming pores) in order to enable cell penetration, similar to what has been proposed for passively transported nanomaterials.[32,39]

Phospholipids are the major component of all cellular membranes. Synthetic bilayer lipid membranes (BLMs) therefore constitute an ideal model system to investigate the physiochemical interactions between nanomaterials and the cell membrane.[40,41] Unmodified BLMs can be easily prepared in solution either as three-dimensional vesicles and liposomes or as two-dimensional supported or free-standing (planar) structures.[34,40] These highly reproducible lipid assemblies have produced much of the available information on biomembranes and their interactions with biological and synthetic objects.[40] Spectroscopic and surface-probe techniques on BLMs have elucidated mechanisms regarding the fluidity and structural rearrangement of the bilayer in response to biomodifiers and nanomaterials, and many models have been successfully used to describe the electrical and physical behavior of BLMs.[40,42,43]

Physically, BLMs can be loosely described as liquid-crystalline in state and are self-healing when punctured, composed of two layers of amphiphilic lipids with charged or polar hydrophilic head groups oriented outward to an aqueous solution and long aliphatic tails positioned inward toward each other, forming a highly hydrophobic interior region. Electrically, BLMs are highly resistive and practically impermeable to hydrated ions, due to the difference of the dielectric constant between the inner hydrophobic region and the external aqueous solution.[40] They also carry an inherent capacitance, as ions can accumulate on the BLM surface so that when an external potential difference is applied, layers of opposite charge are separated by less than 10 nm by the high dielectric constant alkyl region.[40] Electrophysiology experiments with planar bilayer lipid membranes (pBLMs) have been broadly employed in order to exploit the variation of pBLMs' electrical properties in response to biological and synthetic modifiers, such as ion channels, proteins, genetic material, and inorganic semiconductors.[44−49]

In BLM capacitance measurement experiments, two chambers are separated by a hydrophobic partition containing a small micrometer-sized aperture.[40,44] The chambers are filled with an electrolytic solution (50 mM KCl), and electrodes are connected to each chamber. A lipid solution is then painted across the aperture in order to form a pBLM. A potential is applied (clamped) across the membrane, and the resulting current response is amplified and recorded. At this point, biomembrane modifiers can be doped into the pBLM by dissolution of the modifier into the chamber solution or through fusing previously synthesized liposomes containing the modifier of interest. This technique has allowed for precisely controlled single-molecule studies of ion channels and other membrane proteins.[44,46]

In this study, we introduce a simple electrical measurement of pBLMs that can be used to quickly screen the NP/BLM interaction by using the increase in capacitance exhibited by phospholipid bilayers upon the adsorption of nanoparticles (Figure 1). To illustrate the

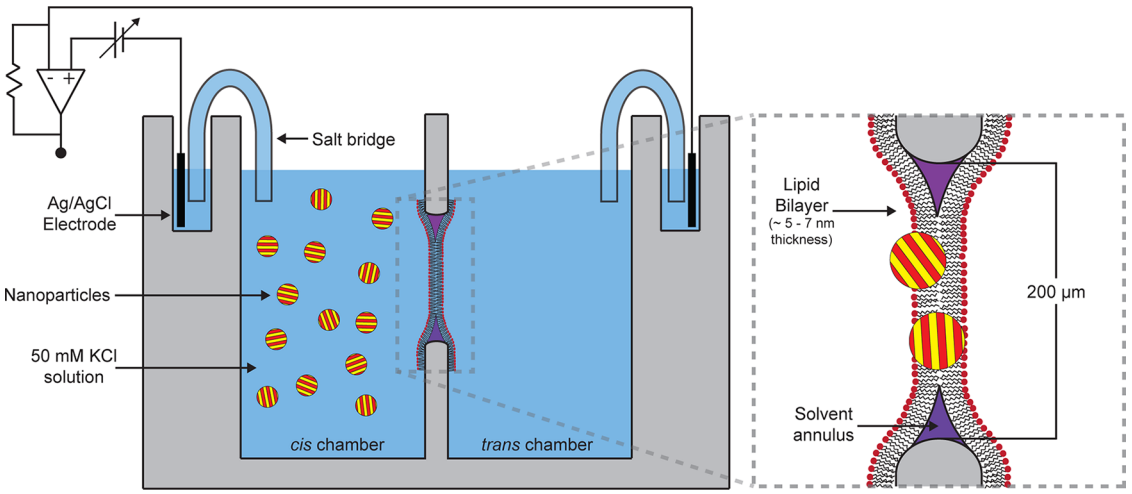

Figure 1. BLM electrophysiology. Two compartments (*cis* and *trans*) are separated by a small aperture that is 200 μm in diameter, onto which the bilayer lipid membrane is formed. The compartments are each filled with an electrolytic solution and connected to electrodes *via* salt bridges. A membrane potential is applied, and the current is amplified using a voltage-clamp amplifier. Increasing concentrations of nanoparticles are then added to the *cis* compartment, and the current/capacitance is monitored by stepped magnitude increases of the square wave due to the insertion of individual NPs into the membrane. Please note that the bilayer thickness and NP diameter are not drawn to scale with respect to the aperture. It is not possible to discern between partially and fully inserted NPs by this method, as reflected in the schematic.

generality of this method, we use a Langmuir model to extract the partition coefficient, K_L, and the standard free energy gain of NP adsorption for a variety of sizes and surface compositions of cell-membrane-penetrating NPs.[21] Finally, we compare these results to *in vitro* studies using flow cytometry and confocal microscopy.

RESULTS

Two types of NPs were used in this study. The first were coated with alternating domains of hydrophobic (octanethiol, OT) and hydrophilic (11-mercaptoundecane sulfonate, MUS) ligands in a molar ratio of 66:34 MUS:OT (hereafter called 66-34OT). These NPs were previously found to passively penetrate cell membranes.[9,21−23] The other type of NP, hereafter referred to as 100MUS, was coated completely with the hydrophilic MUS ligand (Figure 2). 100MUS NPs were previously found to penetrate cells *via* energy-dependent pathways and are consequently used here as a control. Both types of NPs were size-fractionated (see Methods) in order to explore the contribution of NP size to membrane penetration. The size distributions of all fractions were obtained by TEM and AUC measurement.[50] The results of the 66-34OT fractions are shown in Figure 2. The 100MUS fractions were equal in size to the 66-34OT fractions.

Single planar-BLMs can be represented as a plate capacitor in parallel with a resistor.[43] BLMs have a dc resistance (R_m) greater than 10^8 ohm cm^2,[43] which we assumed to remain unchanged during NP adsorption. They can be seen as a parallel-plate capacitor in solution; two polarizable plates composed of the outer surfaces formed by the lipid head groups are separated over a small distance by an insulator, the hydrophobic alkyl BLM interior. BLMs have a characteristic capacitance (C_m) of approximately 0.5 μF/cm^2 when assembled between two aqueous unbuffered solutions of 50 mM KCl.[40] If a voltage is applied across the plates of this capacitor, ions accumulate at the surface of one plate while depleting the other, until the potential between the two plates matches the applied potential. (The parallel drawn between BLMs and the standard plate capacitor is applied loosely here, as the charge carriers in the case of BLMs are ions, not electrons.) Under constant applied potential, current does not flow through the capacitor, yet during charging and discharging, current appears to flow. This charging current is referred to as the capacitive current, I_C.

$$I_C = \frac{dQ}{dt} = \frac{d(CV_C)}{dt} = C\frac{dV_C}{dt} \qquad (1)$$

where Q is the charge on a capacitor plate, C is the capacitance, and V_C is the applied potential. By ramping the transmembrane potential at a constant rate of $\pm$1 V/s, the magnitude of the square-wave current we measure is equal to the capacitance (Figure 3). This approach has the additional advantage that any poration or leakage through the membrane can be identified by the square wave exhibiting a slightly trapezoidal shape or sloped peaks on the plateau. [This assumption was confirmed by artificially creating pores in the membrane by electroporation and observing a transient sloping in the plateau region for the $I-t$ curves. The experimental issue of sloping plateaus is addressed in the Methods section.] The error was taken as one standard deviation of the average plateau value for each trace, representing the electrical noise of the measurement.

We chose two types of lipids in order to form BLMs, 1,2-diphytanoyl-*sn*-glycero-3-phosphocholine (DPhPC) and 1,2-dioleoyl-*sn*-glycero-3-phosphocholine (DOPC).

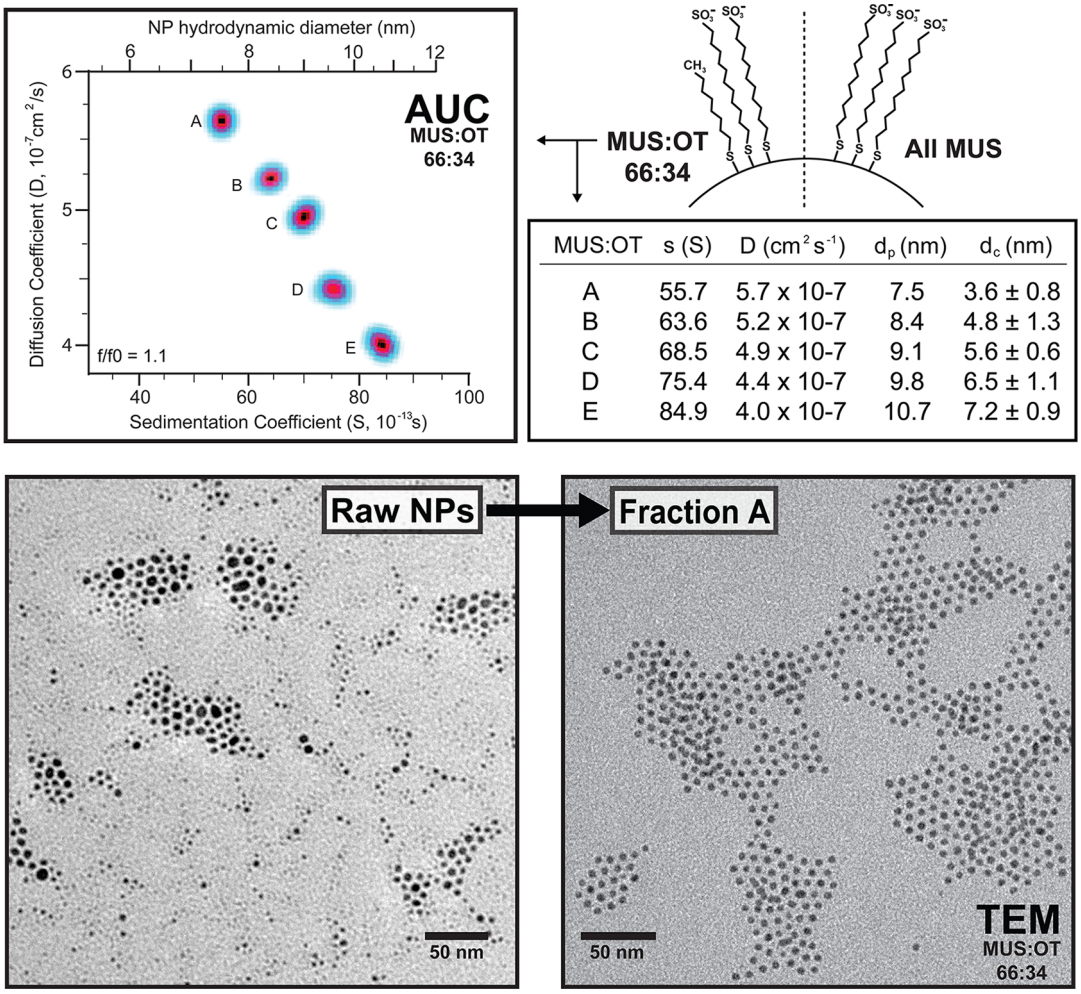

Figure 2. AUC and TEM characterization. Polydisperse all MUS and MUS:OT NPs were both fractionated into five separated fractions. The main MUS:OT AUC peaks are presented together as diffusion coefficients *vs* sedimentation coefficients (with NP hydrodynamic diameter above) (top left). The table lists the AUC-calculated hydrodynamic NP diameter (d_P) and TEM core diameter (d_C) for each of the 5 MUS:OT fractions. The bottom panel shows the TEM micrograph before fractionation (bottom left) and the first population, Fraction A, after fractionation (bottom right).

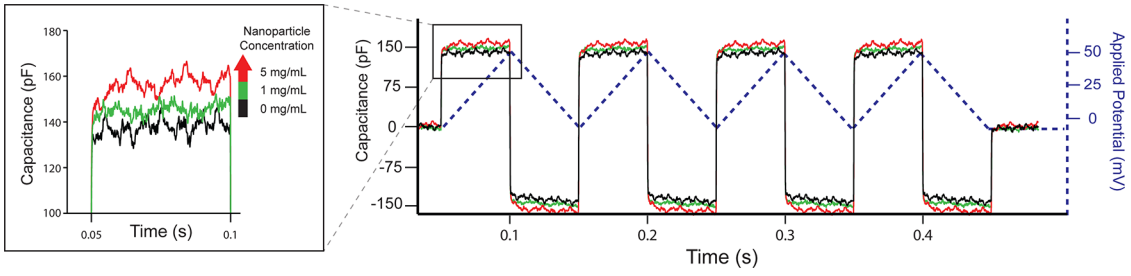

Figure 3. Applied potential and current/capacitive response. Oscilloscope output during a capacitance test. The applied potential (dotted blue line) is ramped linearly between 0 and 50 mV at increments of 50 ms. When the potential is rising, the capacitance value is positive, and when the potential is ramped back down, the capacitance is negative. The magnitude of the capacitance is dependent only on the slope of the potential, not the value. The current/capacitance output square wave is ±138 pA/pF for the unmodified bilayer (black trace) and increases upon adsorption of increasing concentration of NPs (green, 1 mg/mL and red, 5 mg/mL).

Historically, DPhPC has typically been used for BLM experiments due to its high mechanical stability.[40,44] However, DOPC is a better model for representing the fluidity and structure found in typical biological membranes.[51] DOPC is also more commonly used for forming supported-BLMs and vesicles;[51] therefore we also tested the NPs on this system in order to directly compare future work with other types of lipid assemblies, despite the difficulty of forming bilayers. Data presented in Figure 4 were averaged over both DOPC

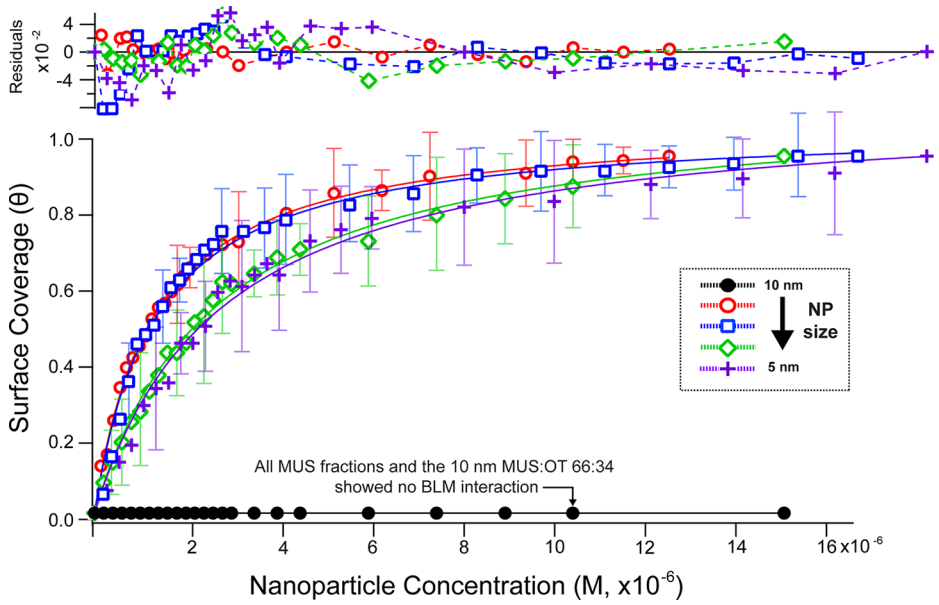

Figure 4. Surface coverage *vs* NP concentration for MUS:OT NP fractions. The surface coverage *vs* NP concentration for each fraction is plotted. The points were fitted with least-squares regression to the adjusted Langmuir adsorption isotherm equation (eq 2.1) to find the adsorption equilibrium constant, K_L. MUS:OT 66:34 fraction A (purple), fraction B (green), fraction C (blue), fraction D (red), fraction E, and all homoligand MUS fractions (black). Each data point represents an average of up to three measurements from different synthetic batches of NP fractions. The error bars represent one standard deviation of the average for repeated measurements. The residuals of the fitted Langmuir adsorption curves are pictured above the data.

and DPhPC lipid membranes. We justify this choice due to their similar chain lengths and fluidity at the temperatures used in these experiments and because we have found no statistically significant difference between NP fusion data collected on both types of membranes. For each experiment, BLMs were formed in a thermocycler at the physiological temperature of 37 °C. After achieving well-formed bilayers with capacitance above a threshold value of 100 pF and no leakage current over a period of 20−30 min, cyclic voltammetry was performed. NP concentration was increased by careful pipet addition, and the solutions were left to equilibrate for 30 min before the capacitance square-wave was recorded. Capacitive increase was typically detected within a few seconds of NP addition and leveled off without change within minutes.

Of the five fractions of 66-34OT NPs, only the largest sized fraction did not interact with BLMs (Figure 4). The remaining four fractions less than 10 nm in diameter were systematically adsorbed into the BLM. The two larger fractions were distinct from the two smaller fractions in adsorption. No single fraction of the 100MUS NPs was adsorbed into the membrane. The change in capacitance plateau magnitude (ΔC) taken from the current traces was recorded with respect to the unmodified bilayer for each increment of NPs added to the *cis* compartment. When plotting the ΔC against the NP concentration (Figure 4), the shapes of the curves follow clear Langmuir adsorption isotherm behavior.[52] We applied this model to extract the Langmuir equilibrium constant, K_L, which can then be used to determine the standard free energy change by the spontaneous NP adsorption (Table 1).[52]

TABLE 1. Data for NP Fractions Adsorbed to BLMs[a]

MUS:OT 66:34		free energy change	
NP fractions	equil. constant K_L (M^{-1})	$\Delta°G \times (k_BT/NP)$	α
A - 7.5 nm	3.6×10^5	−12.8	1.15
B - 8.4 nm	3.8×10^5	−12.9	1.16
C - 9.1 nm	7.8×10^5	−13.6	1.1
D - 9.8 nm	7.6×10^5	−13.5	1.09
E - 10.7 nm			

[a] This table lists the fitted values for equilibrium constants, the calculated values for standard free energy change, and scaling factor, α, for each fraction. The largest 66-34OT fraction, E, and all fractions of 100MUS did not interact with the BLMs. At present we do not have an explanation for why fraction E did not interact with the BLM. We do not know if this was due to the specifics of the interaction of the NPs with the BLM or to a change in surface structure.[53]

The Langmuir isotherm describes the dependence of the surface coverage, θ, of an adsorbed molecule on the concentration of the molecule around the surface at a fixed temperature.[52] A dynamic equilibrium exists between the free NPs in solution and the NPs adsorbed to the BLM. The surface is assumed to have a specific number of sites where the adsorbates can be adsorbed, and these sites are all equally active, giving rise to a single average value of equilibrium constant, K_L. The Langmuir equation gives the relationship between the surface coverage and NP concentration:

$$\theta = \frac{K_L c_{NP}}{1 + K_L c_{NP}} \quad (2)$$

In our experiment, we take the surface coverage, θ, to be the ratio of the change in capacitance with each addition of NPs ($\Delta^i C$) to the maximum change of capacitance when the BLM surface is saturated ($\Delta^i_{max} C$), normalized by the area of that BLM. Unfortunately this condition forces the surface coverage saturation value (plateau value) of each adsorption curve to unity, making it problematic to fit with eq 2, which cannot reach a value of 1. To alleviate this, we added a scaling factor, α, to the Langmuir equation:

$$\theta = \alpha \frac{K_L c_{NP}}{1 + K_L c_{NP}} \quad (2.1)$$

The scaling factor was constrained to be greater than 1 and was iteratively fit for each curve to minimize the rmsd of the fitted line (residuals plotted in Figure 4, top). The physical significance of this parameter is discussed below. We plot the surface coverage, θ, against the concentration and fit the value K_L and α using a least-squares regression (Igor Pro, Wavemetrics, Lake Oswego, OR, USA). We then use K_L to calculate the change of standard free energy during the process.

$$\Delta^\circ G = -RT \ln(K_L) \quad (3)$$

The surface coverage *vs* concentration plots are presented in Figure 4, and the fitted values for K_L, $\Delta^\circ G$, and α are shown in Table 1. NP concentration was converted from mg/mL to molar concentration using the molecular weight for each fraction as determined by AUC.[50] There are two sources of error for this measurement. The first is the experimental error associated with repeating the measurements on different batches of fractions of NPs. The fractionation yield is low compared to the amount of material required to build a complete curve, as pictured in Figure 4, so it was not always possible to repeat measurements on some of the fractions. However most of the concentrations for each fraction were measured multiple times, and this standard deviation was propagated through to error for the surface coverage *vs* concentration plots (Figure 4). Another source of error is the electronic noise for each plateau such as in Figure 3. This noise was lower than the experimental error and is presented for fraction C in Supplemental Figure 2.

Finally, in order to compare the results obtained on BLMs with actual cell membranes, we have tested the same NP fractions as described above for cell penetration in 3T3 fibroblast cells. Our group has previously used these cells to examine cell penetration of surface-structured NPs.[22] The NP fractions were first labeled with a fluorescent dye (BODIPY-SH 630/650) for visualization in confocal laser scanning microscopy (CLSM) and flow cytometry (FC). The experimental details of cell preparation, dye labeling of NPs, and CLSM and FC can be found in the Methods. The results of the cell uptake experiments are presented in Figure 5. Results were also collected at 4 °C in order to satisfy the requirement for non-energy-mediated penetration.

DISCUSSION

The varying sized fractions of NPs coated with 100MUS showed no adsorption behavior, reproducing the surface composition effect found in our previous studies.[9,21−23] Additionally, since only the largest fraction of the 66-34OT NP did not adsorb into the BLM, we can presume the existence of a size cutoff for BLM adsorption. The fractions of 66-34OT NPs that did adsorb exhibited a very similar change in adsorption standard free energy (Table 1), with a slight separation between the two smallest fractions and the two largest fractions. This indicates that within a polydisperse batch of NPs that show cell penetration we can use these electrical experiments to obtain a binary answer as to whether or not the NPs can interact with BLMs and how efficiently they enter in comparison to one another.

It is clearly observable that the Langmuir model used together with the parameter α provides a remarkable fit to the data presented. Yet, we should point out that the Langmuir model requires true reversible adsorption, and a surface should reach full coverage at large concentrations. On multiple occasions, we have tried to observe desorption from the membrane by reducing the concentration of the nanoparticles in solutions after equilibrium was reached at a higher concentration. In no case have we measured a capacitance decrease. In addition, when we fit the adsorption curves to a simple Langmuir, the results are not as great as when we adopt the scaling parameter α. These considerations taken together seem to suggest that once incorporated in the membrane, the particles are very slow in leaving it. Yet, atomic force microscopy data we collected on supported lipid bilayers with these particles strongly suggest large in-lipid particle mobility after fusion.[54] We believe that at low coverage this mobility is equivalent to desorption in a Langmuir treatment, hence the good fit at low concentration independent of α values. At high coverage, lateral mobility is drastically reduced (for simple space consideration), and consequently the absorption becomes kinetically trapped and/or limited. The role of the parameter α is to capture the progressive irreversibility of the adsorption phenomenon. Thus, we think that a fit for a particle/lipid combination with α being 1 would indicate a purely reversible process, and a larger value of α indicates in-lipid mobility but probably lack of true reversibility.

Additionally, one feature of our prediction is that the NPs are inserted into the bilayer and not simply adsorbed onto the surface. We have tested this by introducing NPs to both sides of the membrane, so that if they were simply adsorbing to the surface, the capacitance should double or at least show an increase. In this case we saw no increase in capacitance

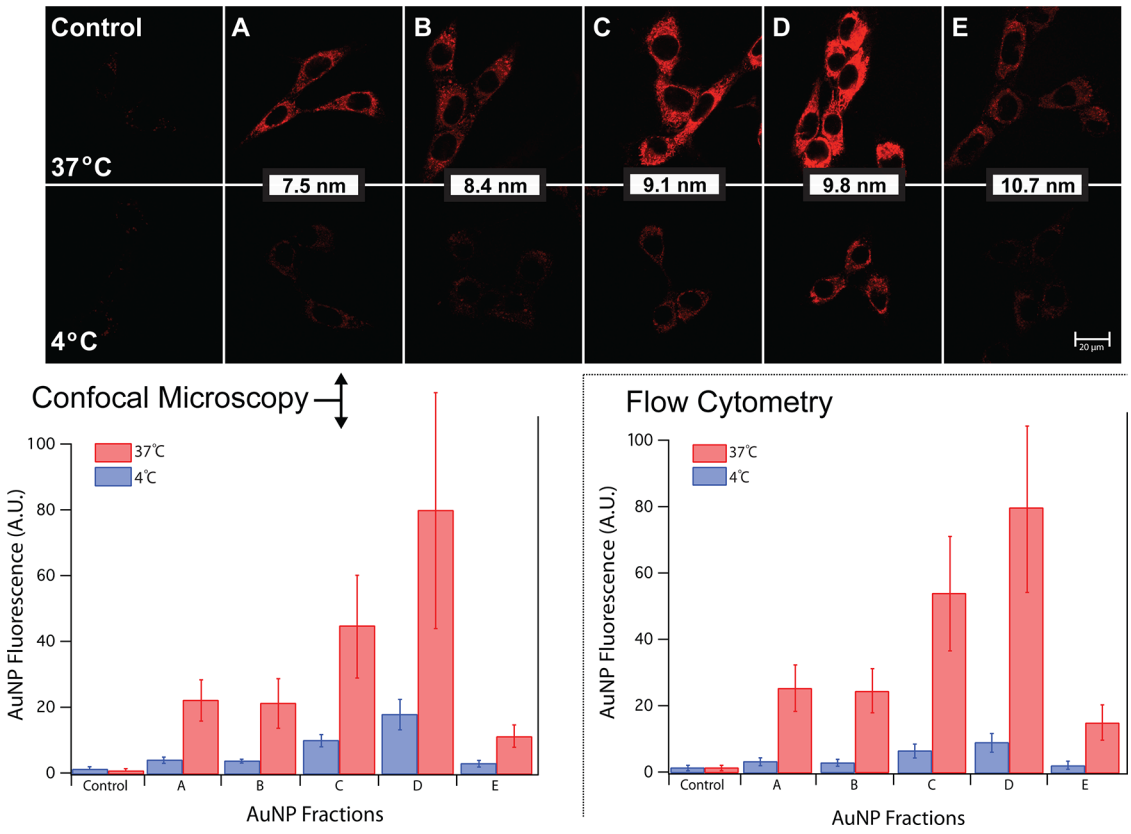

Figure 5. Confocal microscopy and flow cytometry in 3T3 cells after incubation with MUS:OT 66:34 NP fractions. The CLSM data (images/top, quantification/bottom left) are presented for each of the NP fractions increasing in core size (A−E) at both 37 and 4 °C, the latter at which all penetration is non-energy-mediated (>10 cells counted per bar). The FC data quantification (bottom right) confirms the results shown in CLSM (>7500 cells per bar). The figures are displayed with one standard deviation as error bars and show a clear maximum at fraction D. The data have been normalized in fluorescence (*y*-axis).

compared to experiments when the NPs are only introduced to one side of the membrane. In this way we are confident that the NP is inserted into the membrane, but the extent of insertion (partial or full) is unknown (pictured in Figure 1, right). To further prove this, we tested a batch of particles known to fuse with BLMs on a different type of lipid, DMPC, that has a melting transition temperature (T_m) at 23 °C. With the thermocycler, we were able to probe the NP−BLM fusion both below and above the phase transition. The bilayer was formed at 37 °C as usual, and then the temperature was lowered to 15 °C, where the bilayer remained stable. The NPs were added at an intermediate concentration (1 mg/mL). Initially there was no capacitance increase, in contrast to DOPC at this temperature, where the lipids are still above its T_m. We slowly ramped the temperature up. At 19 °C, the capacitance started increasing and eventually stabilized at about 28 °C. If particles were simply adsorbing to the surface of the bilayer, they should remain stable to differences in the lipid phase, but instead they do not adsorb when the bilayer is in gel phase. This supports our conclusion that particles are truly adsorbed into the hydrophobic BLM core. We then tried ramping the temperature back below the T_m to try to observe the NPs' ejection back into solution, but instead the membrane simply became unattached. We will attempt to further address the issue in future spectroscopic and surface probe studies on cell-penetrating NPs with BLMs.

The NPs used in this study are negatively charged, with a measured zeta potential of less than −30 mV. To ensure that application of the electrostatic force did not contribute to the fusion of the NPs and BLMs, both a positive and negative potential (±50 mV) were applied to the *cis* chamber containing the NPs. There was no difference in the magnitude of capacitance change for this control; thus we conclude that the potential of the electrodes did not interfere with the fusion measurements.

The CLSM and FC data confirm the results obtained by electrical measurement of BLMs, with a clear size dependence on cell penetration, maximized at fraction D. However, although the largest fraction, E, never showed adsorption behavior in the electrical measurements, it does show low non-energy-mediated penetration *in vitro*. This result indicates that the model BLM used in our experiments is more selective than the real cell membrane. There are many possible reasons for this, and the most probable lies in the significant compositional difference between BLMs and cell membranes. Nevertheless, the comparable trends derived

with electrical measurements and direct fluorescence measurements in cells strongly support the idea that the electrical method is a suitable platform for achieving fast, systematical, and quantitative screening of nanomaterials susceptible to interactions with cells.

The model remains a rough empirical description, and as with any new phenomenon being experimentally developed, we expect that the quality of data will improve over time. Consequently, the effects of some of the assumptions made above may be eliminated in the future when certain physical aspects are considered, such as a more detailed study of the membranes' structural fluctuations as a result of NP adsorption.[32] Yet we believe that these results show for the first time that there is a driving force for the spontaneous fusion of nanoparticles with lipid bilayers. The standard free energy of the process does not appear to be large ($\sim 13-14 k_B T$) but is certainly sufficient to drive a spontaneous process. Moreover, these values are similar to those found for primary amphipathic CPPs associating with large unilamellar vesicle: $\sim 10 k_B T$ per CPP.[37]

We have shown that we can characterize the NPs' interaction with lipid bilayers from the simplest level of unmodified BLMs up to their penetration into living cells. Additionally, this electrical technique allows for the incremental advancement in complexity to approach increasingly realistic biomembranes. Further work with electrical measurements of BLMs will explore a larger variety of cell-penetrating NPs differing in composition as part of an effort to elucidate a mechanism for cell penetration. We are continuing to develop this technique to also allow the exploration of such effects as membrane swelling or "bowing" out upon fusion with NPs and to understand if NPs are interacting with each other after fusion. We are also exploring the effects on fluidity and membrane structure of the remaining lipid volume after NP fusion. Finally we are planning to develop a complementary optical method to measure the area of the BLM empirically, in order to reduce the error of assuming an area based on the calculated thickness of the lipid bilayer and its theoretical capacitance. This will also allow for the possibility of measuring the physical area represented by the NPs in the bilayer after fusion.

CONCLUSION

In conclusion we have established that a simple low-current measurement amplifier with BLMs as membranes to separate *cis* and *trans* compartments can be used to screen for interactions between NPs and membranes. We also show that these measurements, in conjunction with a simple Langmuir isotherm model, can provide quantitative data for the interaction between lipid bilayers and NPs. Additionally, in this paper we demonstrate that striped-NPs/lipid bilayers spontaneously fuse with a standard free energy of the process of $\sim 14 k_B T$ that is size dependent. We find that striped NPs spontaneously interact with DOPC/DPhPC suspended lipid membranes only if their diameter is smaller than ~10 nm and that similar particles with a homoligand shell do not interact with the same membrane. We hope that this technique will become an important tool to quickly screen the interaction of NPs with BLMs and allow the extraction of some thermodynamic quantities such as the adsorption equilibrium constant and the change in adsorption standard free energy.

METHODS

Planar Bilayer Lipid Membrane Electrophysiology. 1,2-Diphytanoyl-*sn*-glycero-3-phosphocholine and 1,2-dioleoyl-*sn*-glycero-3-phosphocholine were purchased from Avanti Polar Lipids, and *n*-decane was purchased from Fisher Scientific. Lipids were received in chloroform and dried under a stream of nitrogen before being placed under vacuum for several hours to remove all traces of solvent. The lipids were resuspended in *n*-decane to a final concentration of 25 mg/mL and were stored at −20 °C in between use. Bilayers were formed over a 200 μm diameter aperture in a Delrin perfusion cup (Warner Instruments). The lipid/decane solution was generously prepainted on either side of the aperture using a 200 μL plastic pipet tip that had been fire-polished momentarily such that its tip was closed and spherical. The paintbrush and other materials previously in contact with lipid solution were cleaned after each use with Folch solution (chloroform/methanol at a 2:1 ratio). After 30 min of drying the cup was assembled into a thermally conductive chamber and 1 mL of 50 mM KCl solution was added to each side of the aperture. Ag/AgCl electrodes were each connected to small electrode wells also containing 50 mM KCl. These wells were connected to the aperture-adjacent chambers *via* salt bridges containing 3 M KCl and 2% agar. Current and capacitance were measured using the Multiclamp 700B microelectrode amplifier and a CV-7B headstage to connect to the electrodes (Molecular Devices). The data were then acquired through the Axon Digidata 1440A data digitizer (Molecular Devices) at a sampling rate of 150 kHz and analyzed using the Clampex 10.0 software. Signal filtering was performed using the 4-pole Bessel filter built into the amplifier unit, at a setting of 1.6 kHz. The schematic for operation is shown in Figure 1.

In order to check for conductance, we applied a triangle-waveform voltage signal and checked for total conductance. If there was any sign of impedance, the solution was removed and sprayed at the blocked aperture. When total conductance was maintained, the same lipid solution was applied across the outside of the aperture cup (*cis* chamber) by immersing the tip into solution and gently rubbing the tip against the aperture. The formation of a bilayer was indicated by a sharp drop in current and by the formation of a capacitive square waveform. Bilayers were required to reach a capacitance value greater than 100 pF to be used in our experiments. The formation of unmodified BLMs is characteristically difficult, as they break down quite easily with small mechanical or electrical fluctuations. To minimize these effects, all experiments were performed in a Faraday cage (Warner Instruments), a metal box that shields electromagnetic interference. This cage was also placed on a floating air table, typically used for scanning-probe instruments, in order to eliminate mechanical vibrations. These were necessary criteria if one is to ensure consistently high-quality data collection. Frequently, it is difficult to obtain a

defect-free bilayer by the painting method, resulting in sloped peaks on the capacitance *vs* time trace (Supplemental Figure 3). These sloped curves, while useful for those studying molecular transport with channel proteins,[55] are indicative of ionic current flowing. In this case, we assumed our BLM had large defects allowing for solvent flow, and the current we were measuring could no longer be considered solely capacitive. We could make no distinction between defects in the middle of the bilayer or at the edges where the bilayer is "stuck" with hydrocarbon residue. In any case, this necessitated a repainting of the bilayer after removing the defective one with a blast of solvent. If a defect-free bilayer could not be formed in several tries on a single pore, the whole setup was rewashed and dried before trying again.

A typical experiment starts with forming a stable bilayer. Once the capacitance and current remained constant for at least 30 min, a transmembrane potential was cyclically ramped between 0 and 100 mV over 100 ms such that the rate is 1 V/s. A baseline recording was made before adding the nanoparticles to the *cis* chamber. For each NP type, several NP concentration additions (above 5 mg/mL) were first used to find the maximum loading concentration, or plateau value, normalized by area. Then a fresh experiment was performed while the concentration was increased in small increments of 0.1 mg/mL from 0 to 1.5 mg/mL, increasing to 0.25 mg/mL from 1.5 mg/mL until the bilayer broke down (typically around 9−10 mg/mL). Thirty minutes of equilibration was waited in between each NP addition. For recording 60 scans were taken each second over 1 min and averaged together. Sometimes it was very difficult to obtain all of the points in the experiment due to membrane instability and breakdown. Because we measured the maximum loading concentration per membrane area, we can use this value to scale data from multiple bilayers in order to combine the data into a single experiment. This scaling was performed in the software after membrane formation in order to normalize the unloaded membrane capacitance to a single value for each type of NP. This relaxed the need for a single experiment to measure a single adsorption curve and dramatically increased our data collection ability. The entire approach from several capacitance traces to final adsorption curve is illustrated in Supplemental Figure 1 for a typical NP fraction.

Nanoparticle Synthesis. Nanoparticles were prepared according to previous methods.[56] The sulfonate ligand 11-mercaptoundecane sulfonate was synthesized in house according to previous methods.[56] All solvents were purged with nitrogen for 1 h prior to synthesis. All other chemicals were purchased from Aldrich and used without further purification. A 0.9 mmol amount of gold salt ($HAuCl_4$) was dissolved in 150 mL of ethanol. A 0.75 mmol amount of the desired molar ratio of the thiol ligands was dissolved in 20 mL of anhydrous methanol and then added to the gold/EtOH solution. After 5 min, 150 mL of saturated sodium borohydride ($NaBH_4$) in ethanol was added dropwise to the gold/thiol solution. This solution was left to stir for 3 h under nitrogen flow on ice and placed in a refrigerator overnight in order to precipitate the particles. The supernatant was removed and the particles were dried under vacuum overnight and resuspended in aqueous solution. The particles were purified using centrifugal dialysis membranes (MW cutoff of 10 000 Da, Amicon) in order to remove free ligands (as confirmed by ^1H NMR) and further characterized by TEM and AUC.

Nanoparticle Fractionation. We have employed density gradient fractionation of the NPs using a Gradient Station (Biocomp Instruments). This machine is outfitted with both a gradient-forming instrument and a piston-operated fractionator. The linear gradients used for separation were 20−50% w/w sucrose solutions prepared in SW32 centrifuge tubes (38 mL volume). An aqueous NP solution (400 μL, 15 mg/mL) was carefully overlaid on top of each gradient, and six tubes were centrifuged in a Beckmann XL90 ultracentrifuge with SW32 Ti swinging bucket rotor for 2 h at 32 krpm at 20 °C. The samples were manually fractionated *via* piston gradient fractionation, and five 3 mm wide slices were obtained at distances of 8, 12, 16, 20, and 24 mm from the meniscus after centrifugation. The identical fractions from each of the six tubes were combined and purified from sucrose *via* centrifugal filter dialysis. The fractions were analyzed for size and density distributions by AUC (Figure 2).[50]

Flow Cytometry and Confocal Laser Scanning Microscopy. For both flow cytometry (FCM) and confocal laser scanning microscopy, the NPs were labeled with a thiolated fluorescent dye, BODIPY-SH (630/650 nm), according to previous methods.[21,22] 3T3 mouse fibroblasts were used in this study. All CLSM imaging and quantification methods were performed according to methods we have recently published.[22] Briefly, dried NPs were dissolved in milli-Q purified water (1 mg/mL) and filtered to remove precipitates. Cells were plated in eight-well Ibidi μ-slide chambers (IbidiTreat) at a concentration of (1.5−2.0) $\times$ 10^4 cells per well and given fresh serum-containing media after 20−22 h. A final concentration of 0.2 mg/mL for each NP solution was mixed directly in the wells and incubated with the cells for 3 h. The wells were washed three times with serum-containing medium and directly imaged. Confocal images were collected with a Zeiss LSM 700 inverted microscope, using the 63$\times$/1.40 oil objective with a HeNe laser and excitation/emission of 630/650 nm. All images were collected with identical laser settings. For FCM, the 3T3 cells were incubated with the NP solutions and washed once each with media and DPBS (Life Technologies). The cells were detached from the wells with 0.05% Trypsin-EDTA (Life Technologies) and subsequently analyzed with a Beckman Coulter CyAn ADPS flow cytometer using the 640 nm laser.

Conflict of Interest: The authors declare no competing financial interest.

Acknowledgment. The Swiss National Foundation NRP 64 program supported this work. Thanks also to Benjamin H. Wunsch, who began exploring this technique in our lab several years ago.

Supporting Information Available: This information is available free of charge *via* the Internet at http://pubs.acs.org.

REFERENCES AND NOTES

1. Thoren, P. E.; Persson, D.; Esbjorner, E. K.; Goksor, M.; Lincoln, P.; Norden, B. Membrane Binding and Translocation of Cell-Penetrating Peptides. *Biochemistry* **2004**, *43*, 3471–34789.
2. Allen, T. M.; Cullis, P. R. Drug Delivery Systems: Entering the Mainstream. *Science* **2004**, *303*, 1818–18122.
3. Irvine, D. J. Drug Delivery One Nanoparticle, One Kill. *Nat. Mater.* **2011**, *10*, 342–343.
4. Kievit, F. M.; Zhang, M. Cancer Therapy: Cancer Nanotheranostics: Improving Imaging and Therapy by Targeted Delivery across Biological Barriers. *Adv. Mater.* **2011**, *23*, H217–H247.
5. Stark, W. J. Nanoparticles in Biological Systems. *Angew. Chem., Int. Ed.* **2011**, *50*, 1242–1258.
6. Xue, X. J.; Wang, F.; Liu, X. G. Emerging Functional Nanomaterials for Therapeutics. *J. Mater. Chem.* **2011**, *21*, 13107–13127.
7. Ferrari, M. Cancer Nanotechnology: Opportunities and Challenges. *Nat. Rev. Cancer* **2005**, *5*, 161–171.
8. Han, G.; Ghosh, P.; Rotello, V. M. Functionalized Gold Nanoparticles for Drug Delivery. *Nanomedicine* **2007**, *2*, 113–123.
9. Jewell, C. M.; Jung, J.; Atukorale, P. U.; Carney, R. P.; Stellacci, F.; Irvine, D. J. Oligonucleotide Delivery by Cell-Penetrating "Striped" Nanoparticles. *Angew. Chem., Int. Ed.* **2011**, *50*, 12312–12315.
10. Kumari, A.; Yadav, S. K. Cellular Interactions of Therapeutically Delivered Nanoparticles. *Expert Opin. Drug Delivery* **2011**, *8*, 141–151.
11. Lund, T.; Callaghan, M. F.; Williams, P.; Turmaine, M.; Bachmann, C.; Rademacher, T.; Roitt, I. M.; Bayford, R. The Influence of Ligand Organization on the Rate of Uptake of Gold Nanoparticles by Colorectal Cancer Cells. *Biomaterials* **2011**, *32*, 9776–9784.

12. Otsuka, H.; Nagasaki, Y.; Kataoka, K. Pegylated Nanoparticles for Biological and Pharmaceutical Applications. *Adv. Drug. Delivery Rev.* **2003**, *55*, 403–419.
13. Song, B.; Yuan, H. J.; Jameson, C. J.; Murad, S. Permeation of Nanocrystals across Lipid Membranes. *Mol. Phys.* **2011**, *109*, 1511–1526.
14. Roiter, Y.; Ornatska, M.; Rammohan, A. R.; Balakrishnan, J.; Heine, D. R.; Minko, S. Interaction of Nanoparticles with Lipid Membrane. *Nano Lett.* **2008**, *8*, 941–944.
15. Hou, W. C.; Moghadam, B. Y.; Corredor, C.; Westerhoff, P.; Posner, J. D. Distribution of Functionalized Gold Nanoparticles Between Water and Lipid Bilayers as Model Cell Membranes. *Environ. Sci. Technol.* **2012**, *46*, 1869–1876.
16. Ginzburg, V. V.; Balijepailli, S. Modeling the Thermodynamics of the Interaction of Nanoparticles with Cell Membranes. *Nano Lett.* **2007**, *7*, 3716–3722.
17. Chithrani, B. D.; Ghazani, A. A.; Chan, W. C. Determining the Size and Shape Dependence of Gold Nanoparticle Uptake into Mammalian Cells. *Nano Lett.* **2006**, *6*, 662–668.
18. Cho, E. C.; Xie, J.; Wurm, P. A.; Xia, Y. Understanding the Role of Surface Charges in Cellular Adsorption *Versus* Internalization by Selectively Removing Gold Nanoparticles on the Cell Surface with a I2/KI Etchant. *Nano Lett.* **2009**, *9*, 1080–1084.
19. Jiang, W.; Kim, B. Y. S.; Rutka, J. T.; Chan, W. C. W. Nanoparticle-Mediated Cellular Response Is Size-Dependent. *Nat. Nanotechnol.* **2008**, *3*, 145–150.
20. Sandin, P.; Fitzpatrick, L. W.; Simpson, J. C.; Dawson, K. A. High-Speed Imaging of Rab Family Small GTPases Reveals Rare Events in Nanoparticle Trafficking in Living Cells. *ACS Nano* **2012**, *6*, 1513–1521.
21. Verma, A.; Uzun, O.; Hu, Y.; Han, H. S.; Watson, N.; Chen, S.; Irvine, D. J.; Stellacci, F. Surface-Structure-Regulated Cell-Membrane Penetration by Monolayer-Protected Nanoparticles. *Nat. Mater.* **2008**, *7*, 588–595.
22. Carney, R. P.; Carney, T. M.; Mueller, M.; Stellacci, F. Dynamic Cellular Uptake of Mixed-Monolayer Protected Nanoparticles. *Biointerphases* **2012**, *7*, 1–9.
23. Leduc, C.; Jung, J. M.; Carney, R. R.; Stellacci, F.; Lounis, B. Direct Investigation of Intracellular Presence of Gold Nanoparticles *via* Photothermal Heterodyne Imaging. *ACS Nano* **2011**, *5*, 2587–2592.
24. Kostarelos, K.; Lacerda, L.; Pastorin, G.; Wu, W.; Wieckowski, S.; Luangsivilay, J.; Godefroy, S.; Pantarotto, D.; Briand, J. P.; Muller, S.; *et al*. Cellular Uptake of Functionalized Carbon Nanotubes Is Independent of Functional Group and Cell Type. *Nat. Nanotechnol.* **2007**, *2*, 108–113.
25. Dubavik, A.; Sezgin, E.; Lesnyak, V.; Gaponik, N.; Schwille, P.; Eychmüller, A. Penetration of Amphiphilic Quantum Dots through Model and Cellular Plasma Membranes. *ACS Nano* **2012**, *6*, 2150–2156.
26. Verma, A.; Stellacci, F. Effect of Surface Properties on Nanoparticle-Cell Interactions. *Small* **2010**, *6*, 12–21.
27. Ding, H. M.; Tian, W. D.; Ma, Y. Q. Designing Nanoparticle Translocation through Membranes by Computer Simulations. *ACS Nano* **2012**, *6*, 1230–1238.
28. Pogodin, S.; Slater, N. K. H.; Baulin, V. A. Biomolecule Surface Patterning May Enhance Membrane Association. *ACS Nano* **2012**, *6*, 1308–1313.
29. Peetla, C.; Labhasetwar, V. Effect of Molecular Structure of Cationic Surfactants on Biophysical Interactions of Surfactant-Modified Nanoparticles with a Model Membrane and Cellular Uptake. *Langmuir* **2009**, *25*, 2369–2377.
30. Chen, J. M.; Hessler, J. A.; Putchakayala, K.; SPanama, B. K.; Khan, D. P.; Hong, S.; Mullen, D. G.; DiMaggio, S. C.; Som, A.; Tew, G. N.; *et al*. Cationic Nanoparticles Induce Nanoscale Disruption in Living Cell Plasma Membranes. *J. Phys. Chem. B* **2009**, *113*, 11179–11185.
31. Wang, T.; Bai, J.; Jiang, X.; Nienhaus, G. U. Cellular Uptake of Nanoparticles by Membrane Penetration: A Study Combining Confocal Microscopy with FTIR Spectroelectrochemistry. *ACS Nano* **2012**, *6*, 1251–1259.
32. Van Lehn, R. C.; Alexander-Katz, A. Penetration of Lipid Bilayers by Nanoparticles with Environmentally-Responsive Surfaces: Simulations and Theory. *Soft Matter* **2011**, *7*, 11392–11404.
33. Eggeling, C.; Ringemann, C.; Medda, R.; Schwarzmann, G.; Sandhoff, K.; Polyakova, S.; Belov, V. N.; Hein, B.; von Middendorff, C.; Schonle, A.; *et al*. Direct Observation of the Nanoscale Dynamics of Membrane Lipids in a Living Cell. *Nature* **2009**, *457*, 1159–1162.
34. Thompson, T. E.; Sankaram, M. B.; Huang, C. Organization and Dynamics of the Lipid Components of Biological Membranes. *Comp. Physiol.* **2011**, 23–57.
35. Vance, D. E.; Vance, J. E., *Biochemistry of Lipids, Lipoproteins, and Membranes*, 5th ed.; Elsevier Science, 2008.
36. Walter, A.; Gutknecht, J. Permeability of Small Nonelectrolytes through Lipid Bilayer-Membranes. *J. Membr. Biol.* **1986**, *90*, 207–217.
37. Ziegler, A. Thermodynamic Studies and Binding Mechanisms of Cell-Penetrating Peptides with Lipids and Glycosaminoglycans. *Adv. Drug. Delivery Rev.* **2008**, *60*, 580–597.
38. Zorko, M.; Langel, U. Cell-Penetrating Peptides: Mechanism and Kinetics of Cargo Delivery. *Adv. Drug Delivery Rev.* **2005**, *57*, 529–545.
39. Herce, H. D.; Garcia, A. E. Molecular Dynamics Simulations Suggest a Mechanism for Translocation of the HIV-1 Tat Peptide across Lipid Membranes. *Proc. Natl. Acad. Sci. U. S. A.* **2007**, *104*, 20805–20810.
40. Tien, H. T.; Ottova-Leitmannova, A. *Membrane Biophysics: As Viewed from Experimental Bilayer Lipid Membranes*. Elsevier: New York, 2000; Vol. 5.
41. Kunitake, T. Synthetic Bilayer-Membranes - Molecular Design, Self-Organization, and Application. *Angew. Chem., Int. Ed. Engl.* **1992**, *31*, 709–726.
42. Gu, L. Q.; Wang, L. G.; Xun, J.; Ottova-Leitmannova, A.; Tien, H. T. A New Method for the Determination of Electrical Properties of Supported Bilayer Lipid Membranes by Cyclic Voltammetry. *Bioelectrochem. Bioenerg.* **1996**, *39*, 275–283.
43. Wiegand, G.; Arribas-Layton, N.; Hillebrandt, H.; Sackmann, E.; Wagner, P. Electrical Properties of Supported Lipid Bilayer Membranes. *J. Phys. Chem. B* **2002**, *106*, 4245–4254.
44. Tien, H. T. Cyclic Voltammetry of Bilayer Lipid-Membranes. *J. Phys. Chem.* **1984**, *88*, 3172–3174.
45. Wagner, A. J.; May, S. Electrostatic Interactions across a Charged Lipid Bilayer. *Eur. Biophys. J.* **2007**, *36*, 293–303.
46. Tong, Y.; Han, X.; Song, Y.; Jiang, J.; Wang, E. Characterization and Property of DNA Incorporated Bilayer Lipid Membranes. *Biophys. Chem.* **2003**, *105*, 1–9.
47. Chandler, E. L.; Smith, A. L.; Burden, L. M.; Kasianowicz, J. J.; Burden, D. L. Membrane Surface Dynamics of DNA-Threaded Nanopores Revealed by Simultaneous Single-Molecule Optical and Ensemble Electrical Recording. *Langmuir* **2004**, *20*, 898–905.
48. Astier, Y.; Datas, L.; Carney, R.; Stellacci, F.; Gentile, F.; DiFabrizio, E. Artificial Surface-Modified Si3N4 Nanopores for Single Surface-Modified Gold Nanoparticle Scanning. *Small* **2011**, *7*, 455–459.
49. Ramachandran, S.; Merrill, N. E.; Blick, R. H.; van der Weide, D. W. Colloidal Quantum Dots Initiating Current Bursts in Lipid Bilayers. *Biosens. Bioelectron.* **2005**, *20*, 2173–2176.
50. Carney, R. P.; Kim, J. Y.; Qian, H.; Jin, R.; Mehenni, H.; Stellacci, F.; Bakr, O. M. Determination of Nanoparticle Size Distribution Together with Density or Molecular Weight by 2D Analytical Ultracentrifugation. *Nat. Commun.* **2011**, *2*, 335–338.
51. Tabares, J. S. F.; Blas, M. L.; Sereno, L. E.; Silber, J. J.; Correa, N. M.; Molina, P. G. Electrochemistry in Large Unilamellar Vesicles. The Distribution of 1-Naphthol Studied by Square Wave Voltammetry. *Electrochim. Acta* **2011**, *56*, 10231–10237.
52. Butt, H.; Graf, K.; Kappl, M. In *Physics and Chemistry of Interfaces*, Wiley-VCH, 2003.
53. Carney, R. P.; DeVries, G. A.; Dubois, C.; Kim, H.; Kim, J. Y.; Singh, C.; Ghorai, P. K.; Tracy, J. B.; Stiles, R. L.; Murray, R. W.; *et al*. Size Limitations for the Formation of Ordered Striped Nanoparticles. *J. Am. Chem. Soc.* **2008**, *130*, 798–799.

54. Voitchovsky, K.; Ricci, M.; Carney, R. P.; Stellacci, F. Untitled Surface Probe and QCM-D Study of Cell-Penetrating Nanoparticles and Supported Lipid Bilayers. Manuscript in preparation.
55. Wong, D.; Jeon, T.; Schmidt, J. Single Molecule Measurements of Channel Proteins Incorporated Into Biomimetic Polymer Membranes. *Nanotechnology* **2006**, *17*, 3710–3717.
56. Uzun, O.; Hu, Y.; Verma, A.; Chen, S.; Centrone, A.; Stellacci, F. Water-Soluble Amphiphilic Gold Nanoparticles with Structured Ligand Shells. *Chem. Commun.* **2008**, 196–198.